

# COMPUTATION OF UPPER AND LOWER BOUNDS IN LIMIT ANALYSIS USING SECOND-ORDER CONE PROGRAMMING AND MESH ADAPTIVITY

H. Ciria and J. Peraire

*Massachusetts Institute of Technology, Cambridge, MA 02139*

*hciria@mit.edu, peraire@mit.edu*

## Abstract

An efficient procedure to compute strict upper and lower bounds for the exact collapse multiplier in limit analysis is presented. The approach consists of two main steps. First, the continuous problem, under the form of the static principle of limit analysis, is discretized twice (one per bound) using particularly chosen finite element spaces for the stresses and velocities that guarantee the attainment of an upper or a lower bound. The second step consists of solving the resulting discrete nonlinear optimization problems. Towards this end, they are reformulated as second-order cone programs, which allows for the use of primal-dual interior point methods that optimally exploit the convexity and duality properties of the limit analysis model. To benefit from the fact that collapse mechanisms are typically highly localized, a novel method for adaptive meshing is introduced based on decomposing the total bound gap as the sum of positive elemental contributions from each element in the mesh. Additionally, stand-alone computational certificates that allow the bounds to be verified independently, without recourse to the original computer program, are also provided. The efficiency of the methodology is illustrated with applications in plane stress and plane strain, demonstrating that it can be used in complex, realistic problems.

## Introduction

Limit analysis is relevant in many practical engineering areas such as the design of mechanical structures or the analysis of soil mechanics. Assuming a rigid, perfectly-plastic solid subject to a static load distribution, the problem of limit analysis consists of finding the minimum multiple of this load distribution that will cause the body to collapse. This *collapse multiplier* results from solving an infinite dimensional saddle point problem, where the internal work rate is maximized over an admissible convex set of stresses -defined by a yield condition- and minimized over the linear space of kinematically admissible velocities for which the external work rate equals the unity. This saddle point problem embeds the well-known convex (and equivalent) static and kinematic principles of limit analysis (Christiansen, 1981). The presence of the yield condition introduces nonlinearity in the problem, which represents an added difficulty.

Traditionally, the way to overcome this difficulty was to linearize the convex yield condition. With this linearization, first introduced in (Maier, 1970), the resulting problem reduces to a classical linear program (LP). Initially, the LP was solved using the Simplex method (Anderheggen and Knöpfel, 1972; Capurso, 1971; Christiansen, 1981) and, more recently, using Interior Point Methods (IPM) (Andersen and Christiansen, 1995; Christiansen and Kortanek, 1991). The first successful attempts to solve for the exact convex yield condition on fine grids were reported in (Andersen *et al.*, 1998), where the kinematic principle was discretized and then formulated as

a Minimization of Sum of Norms (MSN) subject to a linear constraint. Finally, the discrete problem was solved extending the ideas of IPMs for LP to the MSN. The approach, however, required the use of very cumbersome divergence-free elements when dealing with incompressible problems. This was overcome in (Christiansen and Andersen, 1999), by simultaneously approximating the static and kinematic principles with a discrete duality problem that was solved using the method reported in (Andersen and Christiansen, 1998). This work was further improved in (Christiansen and Pedersen, 2001), by introducing automatic mesh refinement and using the primal-dual IPM developed in (Andersen *et al.*, 2000). Unfortunately, the refinement strategy did not rely on rigorous local error measures but in heuristic estimates, thereby limiting its performance. A common feature of the above-mentioned works, (Andersen *et al.*, 1998; Christiansen and Andersen, 1999; Christiansen and Pedersen, 2001), is that they only provide approximations to the collapse multiplier, but do not yield strict bounds. In (Lyamin and Sloan, 2002a; Lyamin and Sloan, 2002b), on the other hand, lower and upper bounds of the collapse multiplier are computed for soil mechanics problems on uniform meshes, using linear finite elements and a nonlinear two-stage, quasi-Newton optimization algorithm. The method does not require the linearization of the yield condition, but can only handle smooth yield surfaces. A new approach to obtain lower bounds is presented in (Krabbenhoft and Damkilde, 2003). It uses an IPM that exploits convexity and duality, and no particular finite element discretization or yield criterion is required. However, no measure of the error is available, since only lower bounds are obtained.

The main objective of the present work is to devise an efficient and robust method to compute upper and lower bounds, for the exact convex yield condition. Towards this end, the convex nature of the limit analysis problem is exploited by solving the resulting optimization problems using standard conic programming (primal-dual) interior point algorithms. Additionally, mesh adaptive procedures, based on local error measures, are incorporated. Finally, the method provides stand-alone certificates that document the computational results and can be used *a posteriori* to prove its correctness.

## The Limit Analysis Problem. Duality and Exact Bounds

Let  $\Omega$  denote the domain of study, over which  $\mathbf{u} = \mathbf{u}(\mathbf{x})$ , with  $\mathbf{x} \in \Omega$ , represents a plastic velocity or flow field that belongs to a space  $Y$  of kinematically admissible velocity fields. Likewise, let  $\boldsymbol{\sigma} = \boldsymbol{\sigma}(\mathbf{x})$  be a stress field belonging to an appropriate space of symmetric stress tensors  $X$  (see (Christiansen, 1996) for the mathematical requirements on  $Y$  and  $X$ ). If the bilinear form  $a(\boldsymbol{\sigma}, \mathbf{u})$  and the linear form  $F(\mathbf{u})$  denote the well-known *internal* and *external work rates*, respectively, then the equilibrium equation can be expressed by the principle of virtual work, as follows:

$$a(\boldsymbol{\sigma}, \mathbf{u}) = F(\mathbf{u}), \quad \forall \mathbf{u} \in Y. \quad (1)$$

Furthermore, the yield condition is forced by imposing the stress tensor  $\boldsymbol{\sigma}$  to belong to a convex set,  $B$ , of admissible stresses for the material:

$$\boldsymbol{\sigma}(\mathbf{x}) \in B, \quad \forall \mathbf{x} \in \Omega. \quad (2)$$

Our computational treatment of the limit analysis problem exploits the convexity properties of  $B$  and requires, also, that  $B$  can be written in the generic form:

$$B = \{\boldsymbol{\sigma} \in X \mid \sum_k f_k^2(\sigma_{ij}) \leq f_0^2(\sigma_{ij}, q)\}, \quad (3)$$

where  $f_k$  and  $f_0$  are affine functions of their arguments and  $q$  is a constant depending on the material properties. For example, the von Mises yield condition in two and three dimensions, as well as the Mohr-Coulomb and the Tresca yield criteria in plane strain, can be expressed in the form (3).

Now, defining  $C = \{\mathbf{u} \in Y \mid F(\mathbf{u}) = 1\}$ , the exact collapse multiplier,  $\lambda^*$ , results from solving any of the following problems:

$$\lambda^* = \sup \lambda \quad \text{s.t.} \begin{cases} \exists \boldsymbol{\sigma} \in B \\ a(\boldsymbol{\sigma}, \mathbf{u}) = \lambda F(\mathbf{u}), \forall \mathbf{u} \in Y \end{cases} \quad (4)$$

$$= \sup_{\boldsymbol{\sigma} \in B} \inf_{\mathbf{u} \in C} a(\boldsymbol{\sigma}, \mathbf{u}) \quad (5)$$

$$= \inf_{\mathbf{u} \in C} \sup_{\boldsymbol{\sigma} \in B} a(\boldsymbol{\sigma}, \mathbf{u}) \quad (6)$$

$$= \inf_{\mathbf{u} \in C} D(\mathbf{u}). \quad (7)$$

Problem (4) is the so-called *static principle of limit analysis*, whereas (7) is known as the *kinematic principle of limit analysis*. The equality between (5) and (6) follows from strong duality, which is proved in detail in (Christiansen, 1996). Moreover, (Christiansen, 1996) also shows that collapse fields  $\mathbf{u}^*$  and  $\boldsymbol{\sigma}^*$  exist and are a saddle point of  $a(\boldsymbol{\sigma}, \mathbf{u})$ . Indeed, if  $\boldsymbol{\sigma}^*$  and  $\mathbf{u}^*$  are the exact solutions to the static and kinematic principles (4) and (7) respectively, then the following inequalities hold:

$$a(\boldsymbol{\sigma}, \mathbf{u}^*) \leq \lambda^* = a(\boldsymbol{\sigma}^*, \mathbf{u}^*) \leq a(\boldsymbol{\sigma}^*, \mathbf{u}) \quad \forall \boldsymbol{\sigma} \in B, \forall \mathbf{u} \in C. \quad (8)$$

Rigorous lower bounds for the multiplier  $\lambda^*$  can be obtained by exactly satisfying the equilibrium and membership constraints in the static principle (4), which is equivalent to exactly computing the inner infimum in (5). Analogously, upper bounds arise when the inner supremum in (6) is exactly performed or, equivalently, when  $D(\mathbf{u})$  is exactly computed in the kinematic principle (7). These conditions, sufficient to guarantee the attainment of bounds, will be referred to as *bound conditions*.

Now, let us consider a discretization of  $\Omega$  and choose finite element function spaces  $X_h$  for  $\boldsymbol{\sigma}$  and  $Y_h$  for  $\mathbf{u}$ . Then, the discretized version of the variational continuous limit analysis problem (4-7) reads as follows:

$$\begin{aligned} \lambda_h^* &= \max_{\substack{\exists \boldsymbol{\sigma}_h \in B_h \\ a(\boldsymbol{\sigma}_h, \mathbf{u}_h) = \lambda F(\mathbf{u}_h), \forall \mathbf{u}_h \in Y_h}} \lambda = \max_{\boldsymbol{\sigma}_h \in B_h} \min_{\mathbf{u}_h \in C_h} a(\boldsymbol{\sigma}_h, \mathbf{u}_h) \\ &= \min_{\mathbf{u}_h \in C_h} \max_{\boldsymbol{\sigma}_h \in B_h} a(\boldsymbol{\sigma}_h, \mathbf{u}_h) = \min_{\mathbf{u}_h \in C_h} D_h(\mathbf{u}_h). \end{aligned} \quad (9)$$

The above discrete duality holds for all practical discretizations (see proof in (Christiansen, 1996)). In general, for a given choice of  $X_h \times Y_h$ ,  $\lambda_h^*$  is only an approximation to  $\lambda^*$ , but not a bound. However, when the discrete problem (9) is solved using particular combinations of appropriately-chosen interpolation spaces  $X_h \times Y_h$ , then  $\lambda_h^*$  is

guaranteed to be either a lower bound ( $\lambda_h^{*LB} \leq \lambda^*$ ) or an upper bound ( $\lambda^* \leq \lambda_h^{*UB}$ ) of the true collapse multiplier,  $\lambda^*$ . These are the spaces of interest to obtain bounds. From now onwards, those combination of spaces that allow for the attainment of lower bounds will be named *purely static spaces* and denoted by  $X_h^{LB} \times Y_h^{LB}$ . Analogously,  $X_h^{UB} \times Y_h^{UB}$  will denote those spaces that yield upper bounds and will be named *purely kinematic spaces*. The reason why these spaces yield rigorous bounds is because their use allow for the **satisfaction of the bound conditions**.

## Methodology and Implementation

A brief summary of the methodology and implementation to obtain bounds in practice, for the two-dimensional limit analysis problem, is given next. For brevity, all the mathematical details and proofs, as well as many additional explanations and descriptions have been omitted in this section, but can be found in (Ciria, 2004 (May)). Both the plane stress and the plane strain models are addressed. Regarding the yield condition, the von Mises model has been considered. Its restriction to plane stress ( $B_1$ ) and plane strain ( $B_2$ ) reads as follows:

$$B_1 = \{\boldsymbol{\sigma} \in X \mid (\sigma_{11} - \sigma_{22})^2 + \sigma_{11}^2 + \sigma_{22}^2 + 6\sigma_{12}^2 \leq 2\sigma_y^2\}, \quad B_2 = \{\boldsymbol{\sigma} \in X \mid (\sigma_{11} - \sigma_{22})^2 + 4\sigma_{12}^2 \leq \frac{4}{3}\sigma_y^2\}, \quad (10)$$

where  $\sigma_y$  represents the *yield stress* in simple tension. Notice that both  $B_1$  and  $B_2$  agree with (3). For all the problems considered, only triangular meshes are used.

### Lower Bound Problem

To obtain a lower bound, the use of purely static spaces,  $X_h^{LB} \times Y_h^{LB}$ , is required. For both the plane stress and the plane strain cases, one can show that a possible purely static formulation is the following: use of piecewise discontinuous stresses with linear interpolations within the elements, and approximation of the velocity field by constants on each element together with additional linear interpolations along the inter-element boundaries. After using these spaces to discretize the static principle (4) and introducing some reformulations, the following lower bound problem emerges:

$$\lambda_h^{*LB} \equiv \max \lambda \quad \text{s.t.} \quad \left\{ \begin{array}{l} \overbrace{\left( \begin{array}{ccc} \underline{\underline{A}}^{eq1} & : & \underline{\underline{F}}_h^{eq1} & : & \underline{\underline{0}} \\ \underline{\underline{A}}^{eq2} & : & \underline{\underline{F}}_h^{eq2} & : & \underline{\underline{0}} \\ \underline{\underline{A}}_\delta^{soc} & : & \underline{\underline{0}} & : & \underline{\underline{I}}_\delta \end{array} \right)}^{9 \times E + 1 + 3n \times E} \left( \begin{array}{c} \underline{\underline{\sigma}}_h \\ \lambda \\ \underline{\underline{x}}_\delta^{soc} \end{array} \right) = \left( \begin{array}{c} \underline{\underline{0}} \\ \underline{\underline{0}} \\ \underline{\underline{l}}_\delta^{soc} \end{array} \right) \\ \underline{\underline{\sigma}}_h \text{ free, } \lambda \geq 0, \underline{\underline{x}}_\delta^{soc} \in \mathcal{K} \end{array} \right. \quad \left. \begin{array}{l} m_1 = 2 \times E \\ m_2 = 4 \times (|\mathcal{E}^\mathcal{O}| + |\mathcal{E}^\mathcal{N}|) \\ m_3 = 3n \times E \end{array} \right) \quad (11)$$

where  $n = 5$  for  $\delta = 1$  (plane stress) and  $n = 3$  for  $\delta = 2$  (plane strain),  $|\mathcal{E}^\mathcal{O}|$  and  $|\mathcal{E}^\mathcal{N}|$  are the total number of internal and Neumann edges in the mesh, respectively, and  $E$  is the number of triangular elements. Moreover,  $\underline{\underline{\sigma}}_h$  is a vector collecting all the nodal stress components, whereas  $\underline{\underline{x}}_\delta^{soc}$  is a vector of additional variables introduced to impose the yield condition. Furthermore,  $\mathcal{K} = \mathcal{L}^n \times \dots \times \mathcal{L}^n$  is a cartesian product of  $3 \times E$  Lorentz (or second-order) cones (see (Ben-Tal and Nemirovski, 2001)). The first submatrix equation in (11) imposes elemental equilibrium whereas the second equation forces inter-element equilibrium and compatibility with the Neumann

boundary conditions. Finally, the last equation imposes the yield condition. Thanks to the use of a purely static formulation, the above equations guarantee that both equilibrium and membership to the yield set are satisfied over the whole domain.

### Upper Bound Problem

The upper bound problem also results from discretizing the static principle of limit analysis (4). However, in this case, purely kinematic spaces,  $X_h^{UB} \times Y_h^{UB}$ , are used. Unlike the lower bound problem, different spaces are chosen here to deal with the plane stress and the plane strain models. For the plane stress case, a kinematic formulation is obtained by using constant stresses on each element combined with continuous piecewise linear velocities. For plane strain, on the other hand, the velocities are interpolated using piecewise discontinuous linear spaces, whereas the stresses are approximated with constants on each element and additional linear tractions along the inter-element boundaries. In this last formulation, the introduction of discontinuities in the flow is motivated to permit incompressibility, which is required in the plane strain case. However, to guarantee a kinematically admissible velocity field, the jump in the normal component of the velocities along the element edges must be forced to vanish. Moreover, the contribution of the inter-element discontinuities to the internal work rate must also be explicitly considered. Finally, introducing these spaces into (4), the upper bound problems can be cast as follows:

$$\lambda_h^{*UB} \equiv \max \lambda$$

$$s.t. \left\{ \begin{array}{l} \overbrace{\left( \begin{array}{ccc|c} \underline{\underline{A}}^{eq} & : & -\underline{\underline{F}}_h^{eq} & : & \underline{\underline{0}} \\ \underline{\underline{A}}_1^{soc} & : & \underline{\underline{0}} & : & \underline{\underline{I}}_1 \\ \tilde{\underline{\underline{\sigma}}}_h & \text{free, } \lambda \geq 0, & \tilde{\underline{\underline{x}}}_1^{soc} \in \tilde{\mathcal{K}} \end{array} \right)}^{3 \times E + 1 + 5 \times E} \left( \begin{array}{c} \tilde{\underline{\underline{\sigma}}}_h \\ \lambda \\ \tilde{\underline{\underline{x}}}_1^{soc} \end{array} \right) = \left( \begin{array}{c} \underline{\underline{0}} \\ \tilde{\underline{\underline{b}}}_1^{soc} \end{array} \right) \end{array} \right. \quad \begin{array}{l} m_1 = 2 \times (N - N^D) \\ m_2 = 5 \times E \end{array} \quad (12)$$

for **plane stress** and

$$\lambda_h^{*UB} \equiv \max \lambda$$

$$s.t. \left\{ \begin{array}{l} \overbrace{\left( \begin{array}{ccc|ccc} \tilde{\underline{\underline{A}}}^{eq1} & : & \tilde{\underline{\underline{A}}}^{eq2} & : & -\tilde{\underline{\underline{F}}}_h^{eq} & : & \underline{\underline{0}} & : & \underline{\underline{0}} \\ \tilde{\underline{\underline{A}}}^{soc} & : & \underline{\underline{0}} & : & \underline{\underline{0}} & : & \underline{\underline{0}} & : & \underline{\underline{I}}_2 \\ \underline{\underline{0}} & : & \underline{\underline{A}}^t & : & \underline{\underline{0}} & : & \underline{\underline{I}}^t & : & \underline{\underline{0}} \end{array} \right)}^{3 \times E + 4 \times |\mathcal{E}^O| + 1 + 4 \times |\mathcal{E}^O| + 3 \times E} \left( \begin{array}{c} \tilde{\underline{\underline{\sigma}}}_h \\ \underline{\underline{t}}_h \\ \lambda \\ \underline{\underline{s}} \\ \tilde{\underline{\underline{x}}}_2^{soc} \end{array} \right) = \left( \begin{array}{c} \underline{\underline{0}} \\ \tilde{\underline{\underline{b}}}_2^{soc} \\ \underline{\underline{b}}^t \end{array} \right) \end{array} \right. \quad \begin{array}{l} r_1 = 6 \times E - 4 \times |\mathcal{E}^D| \\ r_2 = 3 \times E \\ r_3 = 4 \times |\mathcal{E}^O| \end{array} \quad (13)$$

for **plane strain**. Here,  $\tilde{\mathcal{K}} = \overbrace{\mathcal{L}^n \times \cdots \times \mathcal{L}^n}^E$  (again,  $n = 5$  for plane stress and  $n = 3$  for plane strain),  $N^D$  is the total number of Dirichlet nodes and  $|\mathcal{E}^N|$ , the number of Dirichlet edges. Moreover,  $\tilde{\underline{\underline{\sigma}}}_h$  collects the elemental components of the stresses,  $\underline{\underline{t}}_h$  is a vector of nodal inter-element tractions, and  $\tilde{\underline{\underline{x}}}_1^{soc}$ ,  $\tilde{\underline{\underline{x}}}_2^{soc}$  and  $\underline{\underline{s}}$  are vectors of additional variables used to impose the yield conditions on the elemental stresses and the internal tractions. For both problems, the first equation approximately forces equilibrium, whereas the remainder ones follow from imposing the von Mises condition.

## Solution of the Bound Problems

The above problems present the canonical form of a Conic Program and, in particular, their level of complexity is that of a Second-order Cone Program (SOCP) (see (Bent-Tal and Nemirovski, 2001) for a complete presentation of Conic Programming). This is important mainly for two reasons. First, it allows for the use of state of the art primal-dual interior point algorithms that have been particularly developed for SOCP and that guarantee global convergence and efficiency in the solution process. Moreover, with these algorithms, not only the above discrete static bound problems are solved, but also their duals, which are discrete versions of the kinematic principle. In this way, collapse fields for the stresses and velocities are simultaneously obtained. Second, the bound problems can be solved using any conic programming optimization package. In particular, the generic conic solvers SeDuMi (Sturm, 2001) and SDPT3 (Tütüncü *et al.*, 2001) are the ones used here. In practice, it is possible to introduce a change of coordinates that substantially reduces the dimensions of the above problems while, at the same time, transforming them into pure SOCPs (Ciria, 2004 (May)).

## Certificates

Thanks to the structure of the bound methods presented here, a certificate for a lower or an upper bound only requires the following data: 1) information about the computational mesh (nodal coordinates and connectivities); 2) feasible values of the variables involved in the bound problem solved. With this information, one can directly obtain or verify bounds without the need for solving any optimization problem. This is so because any purely static or purely kinematic feasible solution to the limit analysis problem results in a lower or an upper bound, respectively.

## Mesh Adaptivity

The underlying idea of mesh adaptivity is to efficiently refine the computational mesh,  $\mathcal{T}_h$ , by only dividing the elements that contribute more to the numerical error. In this case, the numerical error is measured by the *bound gap*,  $\Delta_h = \lambda_h^{*UB} - \lambda_h^{*LB}$ . It turns out that it is possible to identify the contribution of each element,  $e$ , in the mesh to the total bound gap. For both the plane stress and the plane strain cases, this contribution, named *elemental bound gap*, is given by

$$\Delta_h^e = \underbrace{\int_{\Omega^e} \sigma_y \varepsilon_{eq}(\mathbf{u}_{UB}^e)}_{D^e(\mathbf{u}_{UB}^e)} - \underbrace{\left( \int_{\Omega^e} (-\nabla \cdot \boldsymbol{\sigma}_{LB}^e) \cdot \mathbf{u}_{UB}^e dV + \int_{\partial\Omega^e} (\mathbf{n}^{\xi_e} \cdot \boldsymbol{\sigma}_{LB}^e) \cdot \mathbf{u}_{UB}^e dS \right)}_{F^e(\mathbf{u}_{UB}^e)}, \quad (14)$$

where  $\boldsymbol{\sigma}_{LB}^e$  is the linear elemental stress tensor computed in the lower bound problem (11) and  $\mathbf{u}_{UB}^e$  are the linear velocities, restricted to the element  $\Omega^e$ , obtained when the upper bound problem (12) or (13) is solved. Moreover,  $\mathbf{n}^{\xi_e}$  is the unit outward normal vector acting on the edge  $\xi_e$  of a particular element and  $\varepsilon_{eq}$  is a scalar deformation known as the *effective strain rate*. Notice that  $\Delta_h^e$  is obtained as the difference between the total elemental energy dissipation rate,  $D^e(\mathbf{u}_{UB}^e)$ , and the elemental external work rate,  $F^e(\mathbf{u}_{UB}^e)$ , both for the upper bound elemental velocity,  $\mathbf{u}_{UB}^e$ . Very conveniently,  $\Delta_h^e$  inherits the following two important properties: 1) It is always positive, i.e.,

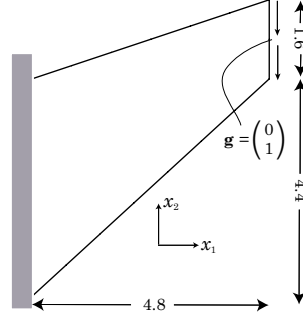


Figure 1: Geometry and loads for the cantilever problem in plane stress

$\Delta_h^e \geq 0, \forall e \in \mathcal{T}_h$ . 2) For plane stress, its sum over all the elements equals the total bound gap, i.e.,  $\sum_{e \in \mathcal{T}_h} \Delta_h^e = \Delta_h$ . For plane strain, the total bound gap is decomposed into two positive terms, namely,  $\Delta_h = \Delta_h^{\mathcal{O}} + \bar{\Delta}_h$ ; where  $\Delta_h^{\mathcal{O}}$  comes from the continuum (interior of the elements) and  $\bar{\Delta}_h$  comes from the inter-element boundaries and is found, in practice, to converge to zero as the mesh is refined, i.e.,  $\bar{\Delta}_h \rightarrow 0$  when  $h \rightarrow 0$ . Then, with the above definition of  $\Delta_h^e$ , the sum of all the elemental bound gaps adds up to the total contribution from the continuum, i.e.,  $\sum_{e \in \mathcal{T}_h} \Delta_h^e = \Delta_h^{\mathcal{O}}$ .

Such  $\Delta_h^e$  is an optimal indicator of the elemental contribution to the numerical error, and refining only the elements with higher  $\Delta_h^e$  is a reasonable strategy to refine the mesh. This is the approach used here.

## Numerical Examples

### *Example 1. Asymmetrical Cantilever in Plane Stress*

In this example, an end-loaded wide tapered cantilever, whose geometry and load distribution are shown in Figure 1, is studied for the plane stress model. Moreover, the performance of the adaptive meshing strategy is compared to the uniform meshing approach. For different computational meshes, the numerical results obtained under each of the two meshing techniques are summarized in Table 1<sup>1</sup>. Notice that, with only 2450 elements, the adaptive meshing yields a maximum relative error of 0.238%, practically the same as the one obtained with 8704 elements when the uniform meshing is used. Moreover, with 5506 elements, the error yielded by the adaptive meshing reduces to 0.066%, which can be considered negligible in practice. Figure 2 illustrates the deformed geometry for different meshes. From a qualitative point of view, the adaptive meshing seems to capture very accurately the collapse mechanism. Indeed, one can observe that the finest elements are aligned in four *slip-lines* that converge in a *plastic-hinge* and that divide the cantilever in four regions. The region in the left-hand side remains fixed, whereas the right-hand side one turns as a solid rigid around the plastic-hinge. This collapse mechanism coincide with the one predicted by the slip-line theory in (Lubliner, 1990) for symmetrical cantilevers.

<sup>1</sup>To compute the relative errors in the table, the exact value  $\lambda^*$  has been assumed to be 0.68504, which is the average of the upper and lower bounds obtained in the last adaptive mesh refinement.

Uniform Meshing						
Number of refin.	Number of elem.	Low. Bound $\lambda_h^{*LB}$	Upp. Bound $\lambda_h^{*UB}$	Bound Gap $\Delta_h$	Low. Bound Error (%)	Upp. Bound Error (%)
0	34	0.52186	0.75759	0.23573	23.821	10.591
1	136	0.65432	0.71936	0.06503	4.484	5.010
2	544	0.68079	0.69704	0.01624	0.620	1.752
3	2176	0.68349	0.68983	0.00634	0.226	0.699
4	8704	0.68440	0.68662	0.00223	0.093	0.231

Adaptive Meshing						
Number of refin.	Number of elem.	Low. Bound $\lambda_h^{*LB}$	Upp. Bound $\lambda_h^{*UB}$	Bound Gap $\Delta_h$	Low. Bound Error (%)	Upp. Bound Error (%)
0	34	0.52186	0.75759	0.23573	23.821	10.591
1	90	0.65782	0.71951	0.06169	3.973	5.032
2	300	0.68079	0.69704	0.01625	0.620	1.752
3	882	0.68349	0.68989	0.00640	0.226	0.708
4	2450	0.68440	0.68667	0.00227	0.093	0.238
5	5506	0.68459	0.68549	0.00090	0.066	0.066

Table 1: Numerical results for the cantilever problem in plane stress

Figure 3 shows graphically the bounds obtained for each uniform refinement and, also, the rate of convergence for the bound errors and for the bound gap. Notice that the upper bound error presents a rate of convergence clearly higher than linear. On the other hand, the lower bound error converges linearly in the asymptotic range, despite the initial super-linear convergence. Finally, in Figure 4, the upper and lower bounds computed for each adaptive refinement are plotted, together with a comparison of the performance of the adaptive versus the uniform meshing procedure. Clearly, the adaptive meshing outperforms the uniform refinement, making it possible to obtain more accurate results at a lower computational cost.

*Example 2. Beam Section in Plane Strain*

The collapse of a symmetrical beam section subject to uniform tension is analyzed here assuming plane strain. Figure 5 illustrates the problem, for which no analytical solution is known. The numerical results obtained for both the uniform and the adaptive refinements are given in Table 2. The last column in the table corresponds to the maximum relative error,  $e_h$ , associated with the *predictor* (the average of the upper and lower bounds). Notice that when adaptive meshing is considered, the results improve substantially. For instance, with 4788 elements (after 5 adaptive refinements),  $e_h = 0.464\%$ , which is less than half of the error incurred in the finest uniform mesh, consisting of 6912 elements. Figure 6 shows the deformation of the body at collapse. Recall that, in plane strain, the velocities are interpolated using piecewise discontinuous linear spaces, but are explicitly forced to be kinematically admissible. This can be observed in the figure. Notice also that the adaptive meshes, especially the finest one, indicate that the main plastic deformations are concentrated within a thin region around a  $45^\circ$  inclined line, with origin in the lower right corner

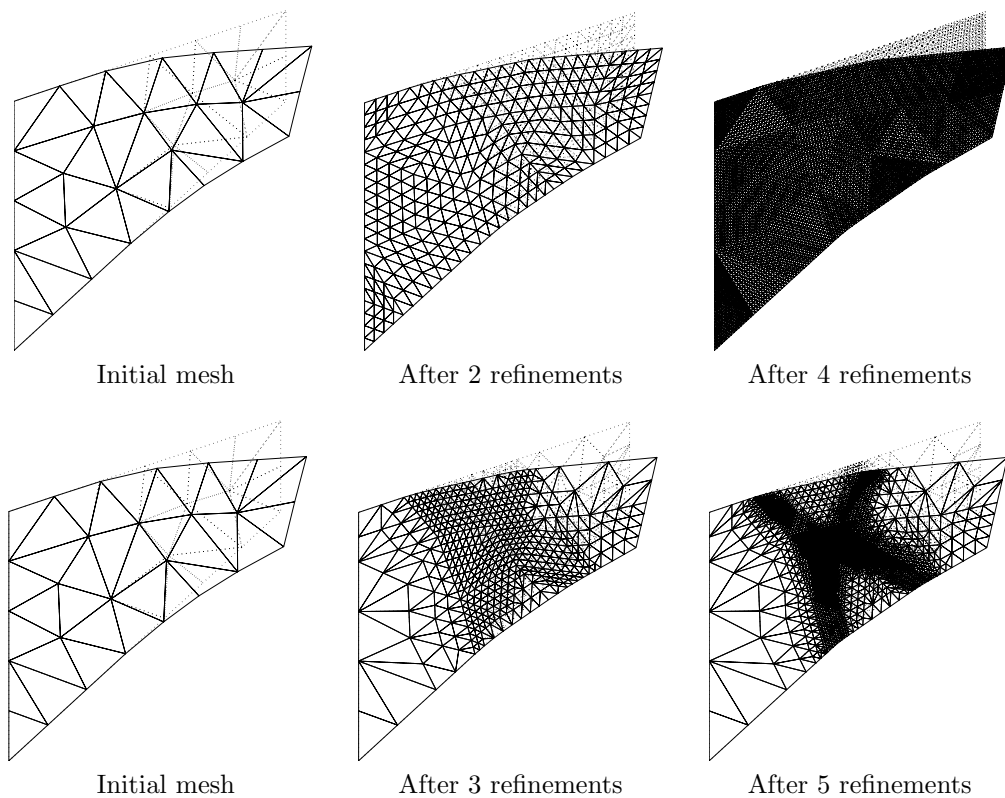


Figure 2: Cantilever problem - Deformed geometry using uniform and adaptive meshing

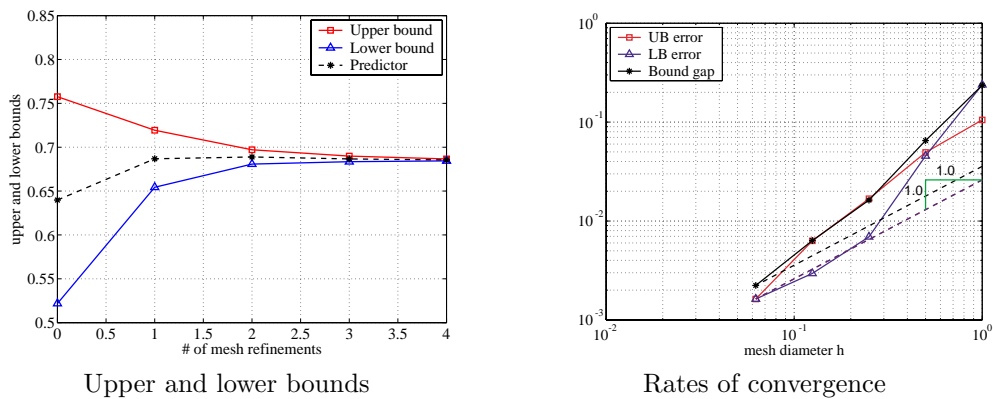


Figure 3: Cantilever problem - Convergence using uniform meshing

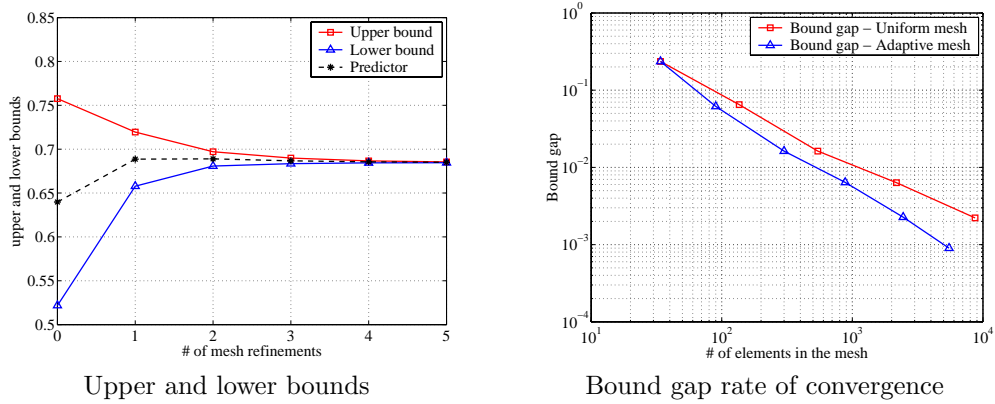


Figure 4: Cantilever problem - Bounds using adaptive meshing and comparison of adaptive versus uniform meshing

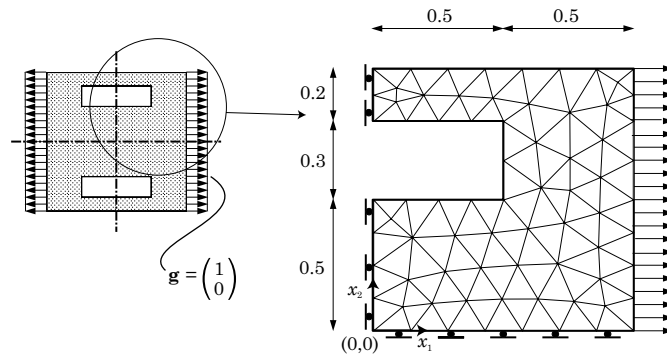


Figure 5: Geometry and loads for the beam section problem in plane strain

Uniform meshing					
Number of refinements	Number of elements	Lower Bound $\lambda_h^{*LB}$	Upper Bound $\lambda_h^{*UB}$	Bound Gap $\Delta_h$	Max. Rel. Error, $e_h$ (%)
0	108	1.2913	1.4151	0.12379	4.574
1	432	1.3195	1.3837	0.06419	2.375
2	1728	1.3215	1.3631	0.04163	1.551
3	6912	1.3219	1.3490	0.02703	1.012

Adaptive meshing					
Number of refinements	Number of elements	Lower Bound $\lambda_h^{*LB}$	Upper Bound $\lambda_h^{*UB}$	Bound Gap $\Delta_h$	Max. Rel. Error, $e_h$ (%)
0	108	1.2913	1.4151	0.12379	4.574
1	251	1.3128	1.3837	0.07088	2.628
2	645	1.3208	1.3632	0.04246	1.582
3	1354	1.3216	1.3493	0.02762	1.034
4	2444	1.3218	1.3402	0.01844	0.693
5	4788	1.3219	1.3342	0.01232	0.464

Table 2: Numerical results for the beam section problem in plane strain

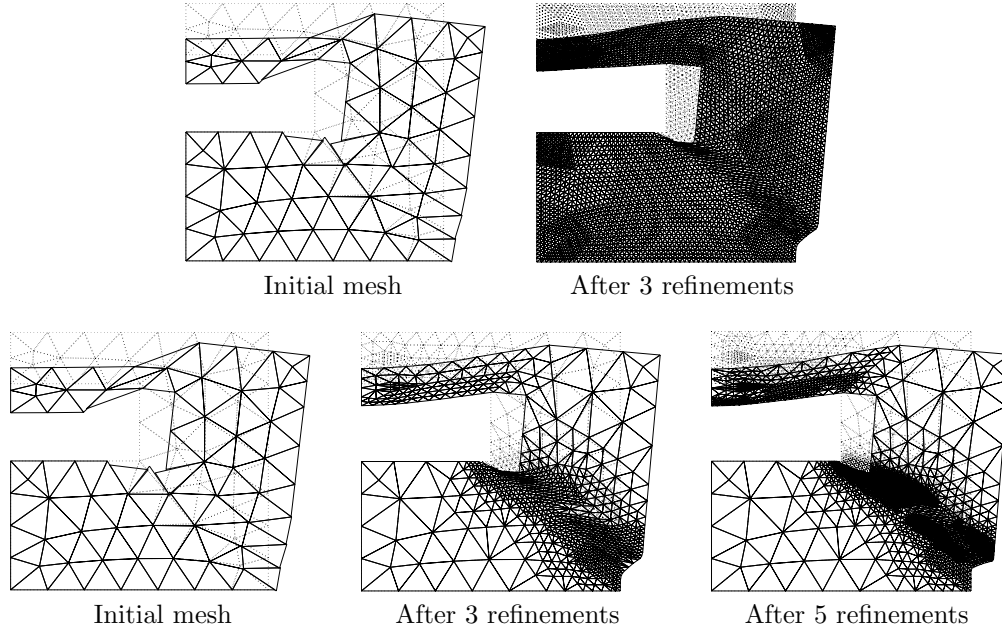


Figure 6: Beam section problem - Deformed geometry using uniform and adaptive meshing

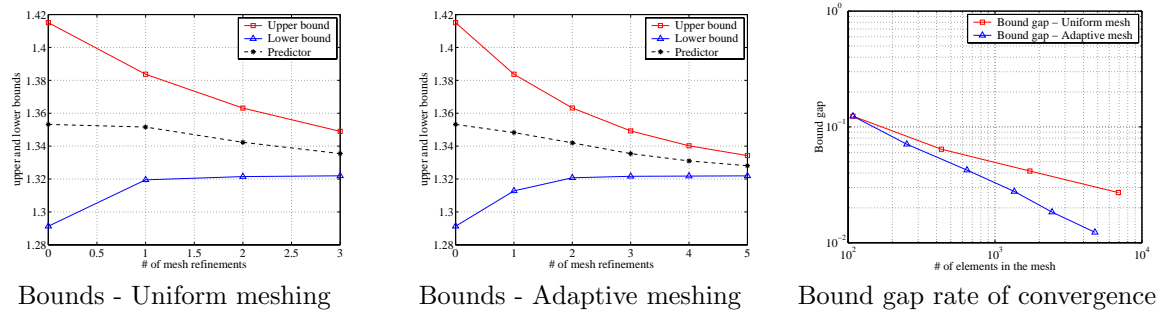


Figure 7: Beam section problem - Convergence using uniform and adaptive meshing

of the interior hole. This plastified region acts as a slip-line over which the upper part of the body flows. Also, some plastic deformations can be encountered in the thin region located over the hole. The adaptive mesh procedure captures very well the plastified regions and concentrates the refinement in those areas.

Finally, Figure 7 illustrates the upper and lower bounds obtained for both the uniform and the adaptive meshings and compares, also, the performance of both approaches. For instance, one can observe that the bound gap resulting from the third adaptive mesh is of the same order as that obtained with the finest uniform mesh. However, in the adaptive case, the mesh has only 1354 elements, much less than the 6912 elements of the uniform mesh. Thus, in the adaptive case, with only 19.6% of the elements, the same accuracy is obtained.

Example	Meshing	# elem.	Lower Bound Problem				Upper Bound Problem		
			# eq.	# var.	SeDuMi	SDPT3	# eq.	# var.	SeDuMi
Ex. 1 Cantilever	unif.	8704	122176	130561	1:57	4:18	52384	69633	0:21
	adap.	5506	77252	82591	1:07	1:27	33120	44049	0:14
Ex. 2 Section	unif.	6912	76432	82945	2:35	10:26	102864	123201	1:31
	adap.	4788	52858	57457	1:51	7:05	71538	85713	0:53

Table 3: Computational cost of solving the bound problems for the finest meshes

### *Computational Cost of Previous Examples*

An indication of the computational cost required to solve the bound problems, for the finest uniform and adaptive meshes used in the two previous examples, is given in Table 3. To solve the problems, the free software SeDuMi 1.05R5 and SDPT3-3.02 was used in Matlab 6.5.1 on a Pentium<sup>®</sup>4 2.53GHz desktop PC. Notice that although SDPT3 is typically slower than SeDuMi, it is also more robust. In (Ciria, 2004 (May)), one can observe that while SDPT3 is always successful at solving the lower bound problem, SeDuMi fails for some examples due to numerical problems.

## Conclusions

To the authors' knowledge, the approach presented in this thesis is the first work that provides a unified framework for computing upper and lower bounds using an efficient formulation and solution process. The efficiency of the methodology mainly derives from the use of IPMs to solve the nonlinear optimization bound problems and, also, from the adaptive meshing technique that is found to capture very accurately the collapse mechanisms. As a consequence, the treatment of rigid-plastic limit analysis (with numerical reliability guaranteed by the obtention of certificates) is ready to be used in real, complex problems as a supplement to other models.

## Acknowledgements

The authors acknowledge the financial support of the Singapore-MIT Alliance and DARPA-AFOSR, through grant F49620-03-1-0439, which made possible the work presented in this article.

## References

- Anderheggen, E., and Knöpfel, H. 1972. Finite element limit analysis using linear programming. *International Journal of Solids and Structures*, **8**, 1413–1431.
- Andersen, K.D., and Christiansen, E. 1995. Limit analysis with the dual affine scaling algorithm. *Journal of Computational and Applied Mathematics*, **59**, 233–243.
- Andersen, K.D., and Christiansen, E. 1998. Minimizing a sum of norms subject to linear equality constraints. *Computational Optimization and Applications*, **11**, 65–79.
- Andersen, K.D., Christiansen, E., and Overton, M.L. 1998. Computing limit loads by minimizing a sum of norms. *SIAM Journal on Scientific Computing*, **19**(3), 1046–1062.

- Andersen, K.D., Christiansen, E., Conn, A.R., and Overton, M.L. 2000. An efficient primal-dual interior-point method for minimizing a sum of euclidian norms. *SIAM Journal on Scientific Computing*, **22**(1), 243–263.
- Ben-Tal, A., and Nemirovski, A. 2001. *Lectures on modern convex optimization: Analysis, algorithms and engineering applications*. SIAM, Philadelphia.
- Capurso, M. 1971. Limit analysis of continuous media with piecewise linear yield condition. *Meccanica - Journal of the Italian Association for Theoretical and Applied Mechanics*, **6**, 53–58.
- Christiansen, E. 1981. Computation of limit loads. *International Journal for Numerical Methods in Engineering*, **17**, 1547–1570.
- Christiansen, E. 1996. *Handbook of Numerical Analysis*. Vol. 4. North-Holland, Amsterdam: In P.G. Ciarlet and J.L. Lions, editors. Chap. Limit analysis of collapse states, pages 193–312.
- Christiansen, E., and Andersen, K.D. 1999. Computation of collapse states with von Mises type yield condition. *International Journal for Numerical Methods in Engineering*, **46**, 1185–1202.
- Christiansen, E., and Kortanek, K.O. 1991. Computation of the collapse state in limit analysis using the LP primal affine scaling algorithm. *Journal of Computational and Applied Mathematics*, **34**, 47–63.
- Christiansen, E., and Pedersen, O.S. 2001. Automatic mesh refinement in limit analysis. *International Journal for Numerical Methods in Engineering*, **50**(6), 1331–1346.
- Ciria, H. 2004 (May). *Computation of upper and lower bounds in limit analysis using second-order cone programming and mesh adaptivity*, M.S. thesis, Massachusetts Institute of Technology, Cambridge, MA 02139.
- Krabbenhoft, K., and Damkilde, L. 2003. A general non-linear optimization algorithm for lower bound limit analysis. *International Journal for Numerical Methods in Engineering*, **56**, 165–184.
- Lubliner, J. 1990. *Plasticity Theory*. Macmillan Publishing Company, New York.
- Lyamin, A.V., and Sloan, S.W. 2002a. Lower bound limit analysis using non-linear programming. *International Journal for Numerical Methods in Engineering*, **55**, 573–611.
- Lyamin, A.V., and Sloan, S.W. 2002b. Upper bound limit analysis using linear finite elements and non-linear programming. *International Journal for Numerical and Analytical Methods in Geomechanics*, **26**, 181–216.
- Maier, G. 1970. A matrix structural theory of piecewise-linear plasticity with interacting yield planes. *Meccanica*, **5**, 55–66.
- Sturm, J.F. 2001. Using SeDuMi 1.02, a Matlab toolbox for optimization over symmetric cones (Updated for version 1.05). Available from <http://fewcal.kub.nl/~sturm>.
- Tütüncü, R.H., Toh, K.C., and Todd, M.J. 2001. SDPT3 - a MATLAB software package for semidefinite-quadratic-linear programming, version 3.0. Available from <http://www.math.cmu.edu/~reha/sdpt3.html>.